

# Ultra-Broadband Wide-Angle Terahertz Absorption Properties of 3D Graphene Foam

Zhiyu Huang, Honghui Chen, Yi Huang,\* Zhen Ge, Ying Zhou, Yang Yang, Peishuang Xiao, Jiajie Liang, Tengfei Zhang, Qian Shi, Guanghao Li, and Yongsheng Chen

As a next generation of detection technology, terahertz technology is very promising. In this work, a highly efficient terahertz wave absorber based on 3D graphene foam (3DG) is first reported. Excellent terahertz absorption property at frequency ranging from 0.1 to 1.2 THz is obtained owing to faint surface reflection and enormous internal absorption. By precise control of the constant properties for 3DG, the reflection loss (RL) value of 19 dB is acquired and the qualified frequency bandwidth (with RL value over 10 dB) covers 95% of the entire measured bandwidth at normal incidence, which far surpasses most reported materials. More importantly, the terahertz absorption performance of 3DG enhances obviously with increasing the incidence while majority of materials become invalid at oblique incidence, instead. At the incidence of 45°, the maximum RL value increases 50% from 19 to 28.6 dB and the qualified frequency bandwidth covers 100% of the measured bandwidth. After considering all core indicators involving density, qualified bandwidth, and RL values, the specific average terahertz absorption (SATA) property is investigated. The SATA value of 3DG is over 3000 times higher than those of other materials in open literatures.

## 1. Introduction

Terahertz radiation (T-ray) usually consists of electromagnetic waves within the frequency ranging from 0.1 to 10 THz.<sup>[1]</sup> In recent years, extensive efforts have been devoted into the development of terahertz science and technology.<sup>[2]</sup> Terahertz imaging,<sup>[3]</sup> terahertz sensors,<sup>[4]</sup> terahertz spectroscopy,<sup>[5]</sup> terahertz high-speed communication,<sup>[6]</sup> and terahertz radar system are all cutting-edge technologies. Among these frontier technologies, terahertz radar, which has higher range resolution, stronger penetrating ability, lower intercept probability, and

better anti-interference ability than microwave radar and infrared detector, gradually attracts more attention. For example, a high-power 215 GHz pulsed radar system was developed for remote-sensing applications at ranges of several kilometers<sup>[7]</sup> and an experimental coherent pulsed radar operating at 225 GHz offered the detection of targets out to ranges of 3.5 km.<sup>[8]</sup>

Generally, terahertz technology is composed of three parts: terahertz sources, terahertz detectors, and terahertz absorbers. While the terahertz sources<sup>[9]</sup> and detectors<sup>[10]</sup> have been developed a lot, there still exists the absence of adequate researches on terahertz absorbers. The thermal detectors, radar systems, electromagnetic shielding, and some other relating things are all in urgent need of the highly efficient terahertz absorbers along with both high terahertz absorption intensity and large qualified bandwidth (reflection loss (RL) larger than 10 dB). Additionally, the

excellent absorption performance at an oblique incident angle is also critical in practical applications.

So far, metamaterials (MMs), which are fabricated by projecting the sub-wavenumber structures of metals (Au, Cu, Al, and so on) and insulators (polyimide) to adjust the conductivity and permeability, are the most investigated materials for terahertz absorbers since they can yield high absorptivity at certain frequencies based on the precise regulation of conductivity and permeability. Most MMs only acquire high absorption performance at a certain frequency,<sup>[11]</sup> but how to realize broadband absorption performance at terahertz frequency range has always been a big challenge. To expand the MMs' qualified bandwidth, the most direct way is to incorporate multiple resonant structures within one-unit cell. Thus, the dual-band terahertz absorbers,<sup>[12]</sup> triple-band terahertz absorbers,<sup>[13]</sup> and even ultra-multi-layer absorbers<sup>[14]</sup> with extremely complicated designs and crafts have been fabricated even though their qualified frequency bandwidths are still hard to reach 80% of the measured frequency range and most of them will lose effectiveness at an oblique incidence. As a result, the disadvantages limit their practical applications.

Carbon-based material with diversified structures, tunable optical properties, and simple preparation methods is another kind of terahertz absorbers. However, the maximum absorption intensities of carbon-based terahertz absorbers, such as

Z. Huang, H. Chen, Prof. Y. Huang, Z. Ge, Y. Zhou, Y. Yang, P. Xiao, Prof. J. Liang, Dr. T. Zhang, Q. Shi, G. Li, Prof. Y. Chen  
National Institute for Advanced Materials  
Tianjin Key Laboratory of Metal and Molecule Based Material Chemistry  
Key Laboratory of Functional Polymer Materials  
Collaborative Innovation Center of Chemical Science and Engineering (Tianjin)  
School of Materials Science and Engineering  
Nankai University  
Tianjin 300071, China  
E-mail: yihuang@nankai.edu.cn

 The ORCID identification number(s) for the author(s) of this article can be found under <https://doi.org/10.1002/adfm.201704363>.

DOI: 10.1002/adfm.201704363

carbon nanotubes (CNTs),<sup>[15]</sup> graphite,<sup>[16]</sup> and graphene,<sup>[17]</sup> are even hard to reach 80%. The strong surface reflection caused by interface mismatch or poor dispersion greatly reduces the terahertz absorption performance. Therefore, how to regulate their electromagnetic properties to enhance terahertz absorption performance is still a challenge. Hence, the terahertz absorbers combining the advantages of high absorption intensity and large qualified bandwidth at wide incident angles is still lacking.

Recently, a significant progress has been made toward the synthesis of 3D graphene.<sup>[18]</sup> Macroscopic 3D graphene foam (3DG) with ultralow density and adjustable optical property has been demonstrated by our group, which may pave the way for the exploitation of graphene as an ultralight, broadband, and wide-angle terahertz absorber.<sup>[19]</sup> Herein, we have first demonstrated the highly efficient 3DG-based terahertz absorber with the density of  $0.8 \text{ mg cm}^{-3}$ . 3DG possesses the maximum RL value of 19 dB at 0.88 THz and the qualified frequency bandwidth covering 95% of the entire measured bandwidth at normal incidence, which is far superior to most of materials reported in open literatures. Moreover, the maximum absorptivity reaches 28.6 dB at 0.64 THz and the qualified frequency bandwidth covers 100% of the measured bandwidth at the incident angle of  $45^\circ$ . Compared with the traditional absorber, such as MMs, graphene oxide (GO), CNTs, and so on, 3DG with highly porous structure possesses stronger absorption intensity, broader qualified bandwidth, and much lower density. The high efficient and broadband absorption performance of 3DG is attributed to the porous structure and the long-rang conductive network. The design of highly porous structure is the key to reduce the surface reflection in contrast to other carbon-based materials as mentioned above, because the efficient dielectric constants of 3DG are well-matched to the dielectric constants of the air. With proper annealing treatment, 3DG could generate

induced currents in the walls while being irradiated. Such long-range-induced currents rapidly attenuate in the resistive network and are converted into thermal energy, which brings about quick decay of massive incident T-ray. Integrating the merits of high absorption, broad bandwidth, and low density, the value of specific average terahertz absorption (SATA) performance for 3DG is over 3000 times higher than those of other materials.

## 2. Results and Discussion

3DG was prepared through the solvothermal method.<sup>[20]</sup> The 3DGs annealed at the different temperatures of 400, 600, 800, 1000, and 1500 °C were abbreviated as T400, T600, T800, T1000, and T1500, respectively. The 3DG without thermal treatment was marked as T0.

The highly porous structure of 3DG has been characterized by scanning electron microscopy (SEM) in Figure 1a,b. The average size of the pore was estimated to about  $42 \mu\text{m}$  in Figure S1 (Supporting Information). And the porosities of 3DGs with different annealing temperatures are above 99.9% (Figure S2, Supporting Information). This distinctive structure plays an important role in absorbing T-ray. The ultrahigh porosity leads to the reduction of the effective dielectric constant. The effective solid contents of the surface are very low, which ensures the majority of incident terahertz radiation irradiated on the surface of the 3DG will enter into the internal with almost no reflection or dispersion.<sup>[21]</sup> The thermogravimetric analyses (Figure 1d) were performed to examine the physicochemical effects of the annealing. T0 appears apparent weight loss when the temperature approaches 200 °C because of the removal of the substantial oxygen-containing functional groups and the mass loss is about 25% at the temperature of 400 °C.

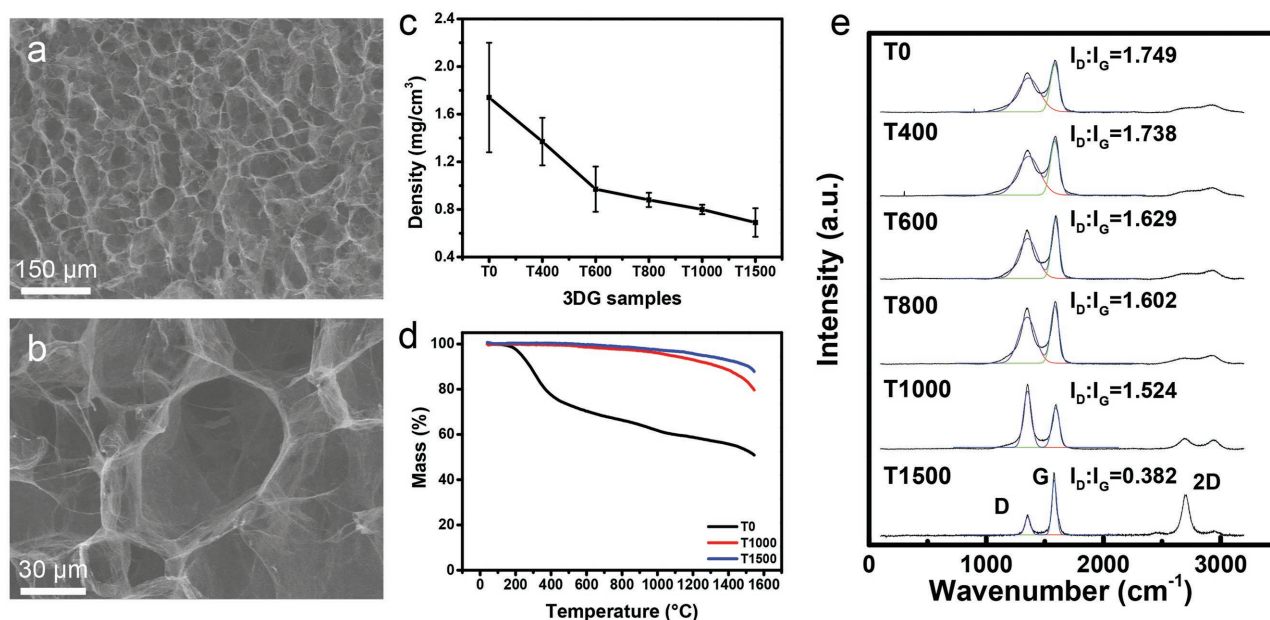


**Figure 1.** a,b) The cross-sectional SEM images of 3DG. c) The densities of 3DGs. d) The thermogravimetric analyses of T0, T1000, and T1500 at  $\text{N}_2$  atmosphere. e) The Raman spectra of 3DG annealed at different temperatures.

For T1000 and T1500 samples, the mass loss significantly decreases compared to the T0 sample because the annealing treatment removes most of the oxygen-containing functional groups and partially restores the conjugated structure of 3DG. The annealing treatment greatly improves the thermal stability for T1000 and T1500. And in the Raman spectra (Figure 1e), 3DG displays two significant peaks at 1350 and 1586  $\text{cm}^{-1}$ , corresponding to the D and G bands, respectively. The area ratio ( $I_D/I_G$ ) is associated with defect concentration of graphitic carbon materials. It can be seen that with the rising of annealing temperature, the  $I_D/I_G$  ratio reduces from 1.749 for T0 to 1.524 for T1000, which demonstrates the enlargement of  $\text{sp}^2$  carbon domain. Furthermore, the  $I_D/I_G$  ratio dramatically decreases to 0.382 for T1500, indicating the large increase of dielectric constants. The half peak widths of both D peak and G peak significantly decrease after 3DG annealing at higher temperature and the 2D peak of 3DG emerges after 1500 °C annealing, suggesting that the graphitization degree greatly increases. With the increase of annealing temperature, the dielectric constants increase significantly (Figures S6 and S7, Supporting Information), which is consistent with the literatures.<sup>[22]</sup> This indicates that the surface reflection and absorption performance would simultaneously increase with the increase of annealing temperature (Figures S8–S10, Supporting Information). In other words, although higher reduction degree generates higher absorption, according to the theory of transmission lines, it also gives rise to higher reflection on the surface of 3DG. And there exists an optimum temperature of thermal treatment for 3DG, which could make 3DG has terahertz absorptivity as much as possible while maintaining low surface reflection.

The terahertz time-domain spectroscopy is a useful method for measuring optical properties of various materials. The terahertz absorption measurement of 3DG over the frequency ranging from 0.1 to 1.2 THz was carried out in a terahertz time-domain spectroscopy system as shown in Figure 2. The aluminum plate is used to reflect the T-ray, which is considered as a nearly total reflection because of the high refractive index of aluminum.<sup>[23]</sup> The first reflected wave from samples and the second reflected wave from aluminum plate are both detected. The lens used to focus the T-ray is placed before the samples. On the condition of the normal incidence

(Figure 2a), the incident T-ray enters the silicon wafer with 200  $\mu\text{m}$  thickness at an angle of 45° and then focuses on the surface of 3DG. The reflected wave is transmitted to the receiver through the silicon wafer. Under the circumstance of the oblique incidence (Figure 2b), the incident angle is tuned by rotating the round platform and precisely adjusting the displacement platform.

Both the annealing temperature and the thickness are critical to the terahertz absorption performance of 3DG. Figure 3a–d gives the RL curves of 3DGs with different thicknesses (1–4 mm) and different annealing temperatures in the frequency range of 0.1–1.2 THz, respectively. The T0 samples with 1–4 mm thickness all exhibit very inferior terahertz absorbing ability in the measured frequency range owing to severe disruption of in-plane conjugated structures of 3DGs. With the increase of annealing temperature, the absorptivity of 3DG is gradually improved, which is consistent with the increase of calculated absorption coefficient and extinction coefficient (Figures S9 and 10, Supporting Information). For example, the maximum value of RL improved from 1 dB for T0 with 4 mm thickness to 16 dB for T800 with 4 mm thickness and the qualified frequency bandwidth for T800 with 4 mm thickness reaches 96% of the measured frequency range (Figure 3d). Then, 3DG annealed at 1000 °C has a better absorptivity and remains a broad qualified frequency bandwidth. For T1000 with 4 mm thickness, the maximum RL value reaches 19 dB at 0.88 THz and the qualified frequency bandwidth reaches 1.045 THz, covering 95% of the entire measured bandwidth (Figure 3d). With the annealing temperature further increasing, the changes of the 3DGs terahertz absorption performance do not maintain a monotonic evolution because a larger surface reflection makes a negative effect on the absorption performance. Upon the annealing temperature reaching 1500 °C, the T1500 samples with different thickness (1–3 mm) all maintain high terahertz absorption performance owing to relative low surface reflection and larger internal absorption. For example, T1500 with 1 mm thickness possesses the maximum RL value of 15.6 dB and its qualified bandwidth ranges from 0.31 to 1.2 THz, covering 81% of the measured frequency (Figure 3a). Considering both absorption performance and the thickness, T1500 owns the best absorption performance among the samples with 1 or 2 mm thickness.

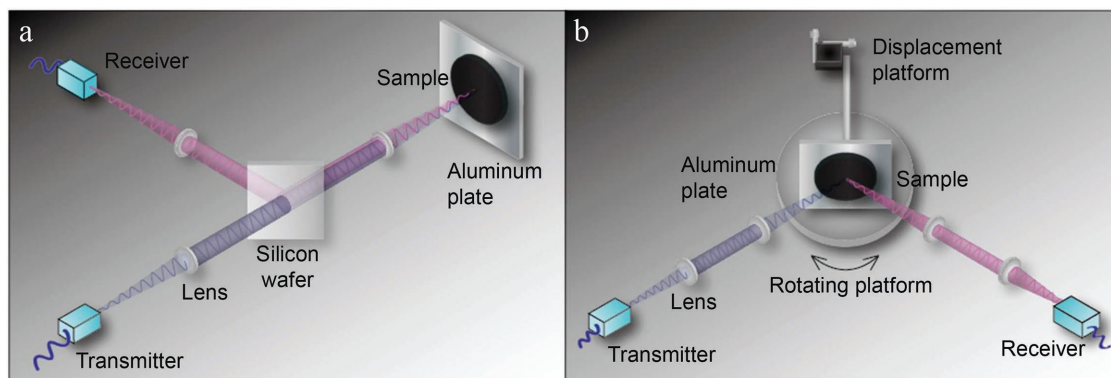


**Figure 2.** Schematic diagram describing a terahertz time-domain spectroscopy system used for terahertz absorption measurements over the frequency from 0.1 to 1.2 THz at a) normal incidence and b) oblique incidence. The blue and red lines refer to the incident wave and the reflected wave, respectively.

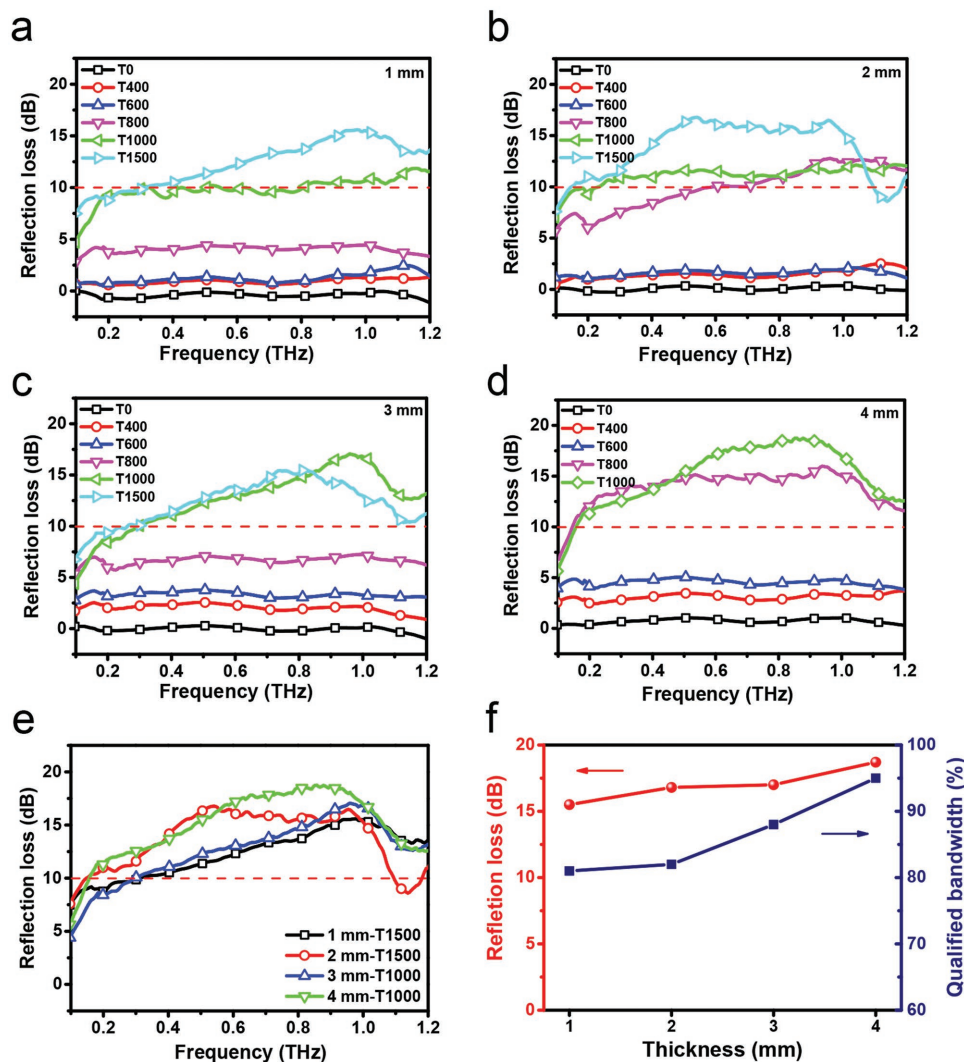


**Figure 3.** The RL curves of original 3DGs and 3DGs with different annealing temperatures (400–1500 °C) with a) 1, b) 2, c) 3, and d) 4 mm thickness. The terahertz absorption performance of T1000 sample with 4 mm thickness is the optimum. e) The RL curves of the best performance for each thickness of 3DG. f) The maximum RL value and qualified bandwidth for each thickness of 3DG.

And T1000 possesses the best absorption performance among samples with 3 or 4 mm thickness (Figure 3e). Both the RL values and the qualified frequency bandwidths for 3DGs with different thicknesses are very outstanding (Figure 3f), which is superior to other materials reported.

The schematic diagram of the propagation of T-ray is shown in Figure 4a. The initial incident T-ray is divided into the multiple reflection, transmission, and absorption

$$I_0 = (I_{R1} + I_{A1} + I_{T1}) + (I_{R2} + I_{A2} + I_{T2}) + \dots + (I_{Rn} + I_{An} + I_{Tn}) \quad (1)$$

where  $I_0$ ,  $I_{Rn}$ ,  $I_{An}$ , and  $I_{Tn}$  respond to the incident terahertz, the  $n_{th}$  order reflection, the  $n_{th}$  order absorption, and the  $n_{th}$  order transmission, respectively. Since the intensities of multiple reflections, such as  $I_{R3}$ , are too weak to be observed, therefore they are not taken into account. And the aluminum plate is considered as a nearly total reflection plane as mentioned above. Therefore, the above equation can be simplified as

$$I_0 = I_{R1} + I_{R2} + I_A \quad (2)$$

As can be seen from Equation (2), absorbers can acquire greater absorptivity by reducing the values of  $I_{R1}$  and  $I_{R2}$  as far as possible. The signals of  $I_{R1}$  and  $I_{R2}$  are all recorded in the terahertz time-domain spectroscopy. In Figure 4b,c, the first signal  $I_{R1}$  and the second signal  $I_{R2}$  are contributed to the surface reflection of 3DGs and the surface reflection of aluminum plate, respectively. The time difference between  $I_{R1}$  and  $I_{R2}$  indicates the thickness and the dielectric constants of different samples. The terahertz time-domain spectroscopies clearly illustrate the intensities of surface reflection and internal absorption of different samples. As shown in Figure 4b, the signal  $I_{R1}$  gradually emerges and increases with the increase of annealing temperature, indicating a larger surface reflection. At the same time, the intensity of  $I_{R2}$  evidently decreases, demonstrating a higher absorption performance, which agrees well with the higher real part and imaginary part

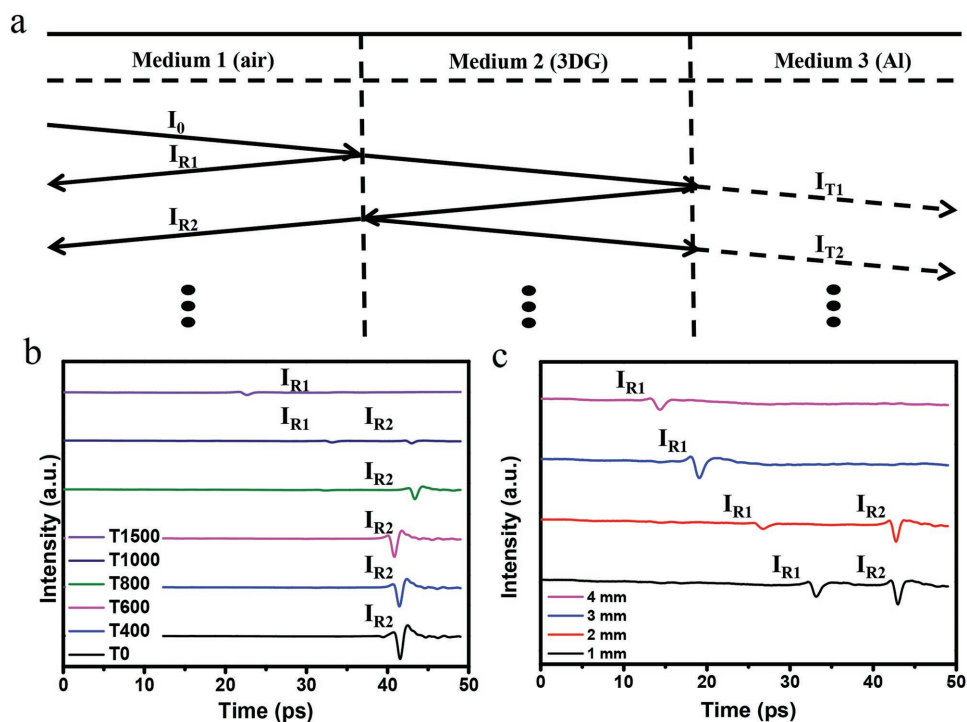


**Figure 4.** a) The schematic diagram of the propagation of T-ray. The signals of  $I_{R1}$  and  $I_{R2}$  are detected from the terahertz time-domain spectroscopy and multiple reflection signals are too weak to be detected. The terahertz time-domain spectroscopy of b) 3DGs with 1 mm thickness under different thermal treatment and c) the T1000 sample with different thickness (1–4 mm).

of dielectric constants (Figures S6 and S7, Supporting Information). For T1000, the signal  $I_{R2}$  almost disappeared, which refers to a very excellent absorption. But for T1500, the signal  $I_{R1}$  increases obviously compared to that of T1000. The results indicate that T1500 has larger surface reflection than that of T1000, which has a negative effect on the terahertz absorption. Therefore, the T1000 sample with 4 mm thickness possesses the best absorption performance since it can absorb the majority of T-ray while maintaining a very low surface reflection. Then the influence of different thicknesses for T1000 is also studied by the time-domain spectroscopy (Figure 4c). With the thickness increasing from 1 to 4 mm for T1000, the intensity of  $I_{R1}$  hardly changes and the intensity of  $I_{R2}$  decreases significantly. It means that the surface reflection of T1000 is almost constant while the internal absorption of incident T-ray is enhanced a lot with the thickness increasing. Therefore, T1000 with 4 mm thickness has the optimal absorption performance.

In most practical applications, T-ray comes from different directions. It is important to maintain excellent absorption performance at oblique incidence. Among the reported terahertz absorbers, their absorptivity and qualified bandwidth both decrease obviously at oblique incidence, in spite that they work well at normal incidence. Instead, the 3DG-based terahertz absorber in the present work has higher absorptivity while the incident angle increasing. The RL curves of T1000 samples with different thickness (1–4 mm) at different incident angles ( $0^\circ$ ,  $30^\circ$ ,  $40^\circ$ , and  $45^\circ$ ) are shown in Figure 5a–d and the absorption performance at larger incident angles was not measured due to the instrumental limitations. The absorptivity and the

qualified frequency bandwidth are surprisingly both improved with the incident angle increasing. For example, the maximum value of RL reaches 28.6 dB at 0.64 THz and the qualified frequency bandwidth covers 100% measured bandwidth at the incident angle of  $45^\circ$ , where the maximum RL value increases by 50% from 19 to 28.6 dB and the average RL value (integrated RL value divided by measured frequency range) increases by 58% from 15 to 23.7 dB compared with the absorption performance at normal incidence. While increasing the incident angle, the absorptivity of 3DG significantly improved due to longer optical distance and larger surface scattering. As described in Figure 5e,f, notably, the qualified bandwidth and the maximum absorptivity of 3DG far surpass those of the reported representative MMs and previous carbon-based materials as mentioned above. Especially, after comprehensive consideration of density, qualified bandwidth, and RL values, the SATA of 3DG is over 3000 times higher than those of traditional materials (Table S1, Supporting Information).

### 3. Conclusion

In summary, we have succeeded in acquiring the wide-angle, large-bandwidth, and high-intensity terahertz absorbers based on foams with porosity of 99.9% and density of  $0.80 \text{ mg cm}^{-3}$ . 3DG is bulk materials with no dispersion problem which often diminishes the absorption performance in the most carbon-based composites. The highly porous structure with 99.9% porosity contributes to low surface reflection because of low efficient dielectric constants. And the annealing treatment

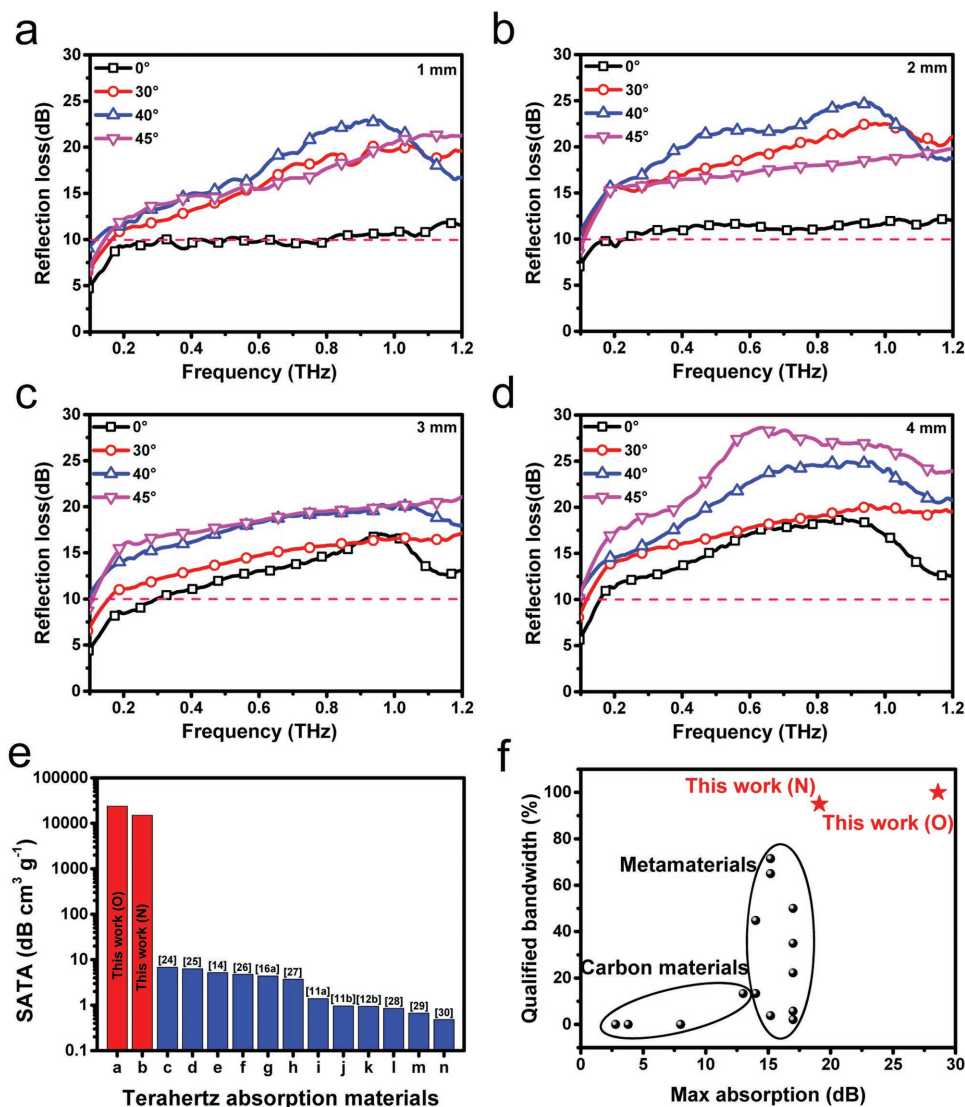


**Figure 5.** The RL curves for T1000 with a) 1, b) 2, c) 3, and d) 4 mm thickness at different incident angles ( $0^{\circ}$ – $45^{\circ}$ ). The maximum value of RL reaches 28.6 dB at 0.64 THz and the qualified frequency bandwidth covers almost 100% of the measured bandwidth at the incident angle of  $45^{\circ}$ . e) Direct comparison of the SATA performance of 3DGs (red) in this work with those of representative materials (blue) in open literatures. f) Direct comparison of the absorption performance of 3DGs (marked as star) in this work with those of traditional terahertz absorbers (marked as pebble), including MMs and carbon-based materials. This work (N) and this work (O) respond to the absorption performance at normal incidence and oblique incidence, respectively.

of 3DGs can further regulate the optical properties to yield a high absorptivity over a wide frequency range. Compared with traditional terahertz absorbers, T1000 with 4 mm thickness delivers a substantially enhanced terahertz absorption performance with the maximum RL value of 19 dB and the qualified frequency bandwidth of 1.045 THz, covering 95% of the entire measured bandwidth at normal incidence. Besides, T1500 samples with different thickness (1–3 mm) all maintain high terahertz absorption performance owing to relative low surface reflection and higher internal absorption. For instance, T1500 with 1 mm thickness possesses the maximum RL value of 15.6 dB and its qualified bandwidth ranges from 0.31 to 1.2 THz, covering 81% of the measured frequency at normal incidence. Remarkably, the 3DG-based terahertz absorber has

much higher absorptivity with the incident angle increasing while the absorptivity and qualified frequency bandwidth of most reported materials both decrease obviously at oblique incidence in spite of the fact that they work well at normal incidence. At the incident angle of  $45^{\circ}$ , the maximum RL value for the T1000 sample with 4 mm thickness even reaches 28.6 dB at 0.64 THz and the qualified frequency bandwidth covers 100% of the measured bandwidth. Finally, the value of SATA performance for 3DG is over 3000 times higher than those of other materials in open literatures. Hence, 3DG as a lightweight, wide-angle, broad-bandwidth, and highly efficient terahertz absorber opens up great opportunities for the next generation of radar detection technique in space, which is a highly important military tool in the future.

## 4. Experimental Section

**Synthesis of Graphene Oxide:** Graphene oxide was prepared by using a modified Hummers method.<sup>[18b]</sup> In brief, flake graphite (10 g, average particle diameter of 300 μm, 99.95% purity, Qingdao Tianhe Graphite Co. Ltd., Qingdao, China) and NaNO<sub>3</sub> (7.5 g, A.R.) were placed in a flask. Then, H<sub>2</sub>SO<sub>4</sub> (750 mL, A.R.) was added with stirring in an ice-water bath, and KMnO<sub>4</sub> (45 g, A.R.) was slowly added over about 0.5 h. Stirring was continued for 1 h in the ice-water bath. Then the product was poured into the beaker and placed in the oven at 60 °C for 6 h. After that they were slowly added into a beaker containing H<sub>2</sub>O of twice volume than the intermediate after returning to the room temperature. When the temperature was reduced to 60 °C, H<sub>2</sub>O<sub>2</sub> (15 mL, 30 wt% aqueous solution) was added. To remove the ions of oxidant and other inorganic impurity, the resultant mixture was purified by repeating the following procedure: centrifugation, removal of the supernatant liquid, addition of H<sub>2</sub>O, and dispersing the solid using vigorous stirring and ultrasonication for 10 min. After complete removal of impurity, centrifugation and addition of ethanol were repeated to obtain graphene oxide which was resolved in ethanol solution.

**Synthesis of 3DG:** 3DG was prepared by solvothermal reaction.<sup>[20]</sup> Briefly, the resultant GO ethanol solution (0.5 mg mL<sup>-1</sup>) was treated in a custom Teflon autoclave at 180 °C for 12 h to form an ethanol-filled intermediate solid. The gradient solution was then applied to replace the internal ethanol with water. After the solvent exchanging, the water-filled intermediate was freeze-dried to remove the remaining water inside. The resultant 3DG was annealed at the different temperatures of 400, 600, 800, 1000, and 1500 °C for 2 h in argon at ramp rate of 5 °C min<sup>-1</sup> separately to obtain the target 3DGs. Finally, 3DGs with 3 cm diameter were cut into 1–4 mm thickness by the laser cutting device with 1.5 W power.

**Measurement of Terahertz Absorption Performance:** The reflection of 3DGs was tested by the terahertz time-domain spectroscopy system (TP15K-F). Both the transmitter and the receiver are commercialized photoconductive antennas. The laser is a femtosecond fiber laser with 1550 nm center wavelength and 50 fs pulse width. The resolution of spectroscopy is less than 3.5 GHz. The 3DGs were adhered closely to the aluminum plate. Both the normal incidence and the oblique incidence were tested using this terahertz time-domain spectroscopy system. The spot size of T-ray focusing on the samples is 0.8 cm diameter.

## Supporting Information

Supporting Information is available from the Wiley Online Library or from the author.

## Acknowledgements

The authors gratefully acknowledge financial support from the MOST (2016YFA0200200), NSFC (21374050, 51373078, and 51422304), and NSF of Tianjin City (15JCYBJC17700). The authors appreciate Prof. J. G. Han, S. X. Li, and Q. Wang (Center for Terahertz Waves of Tianjin University) for their support in the test of terahertz absorption.

## Conflict of Interest

The authors declare no conflict of interest.

## Keywords

broadband, graphene foam, terahertz absorption, wide-angle absorption

Received: August 1, 2017  
Revised: September 24, 2017  
Published online:

- [1] B. Ferguson, X.-C. Zhang, *Nat. Mater.* **2002**, *1*, 26.
- [2] a) P. Dean, A. Valavanis, J. Keeley, K. Bertling, Y. L. Lim, R. Alhathloul, A. D. Burnett, L. H. Li, S. P. Khanna, D. Indjin, T. Taimre, A. D. Rakić, E. H. Linfield, A. G. Davies, *J. Phys. D: Appl. Phys.* **2014**, *47*, 374008; b) Z. Chen, G. Hefferman, T. Wei, *IEEE J. Sel. Top. Quantum Electron.* **2017**, *23*, 246; c) J. B. Eom, C. Kim, J. Ahn, *Opt. Commun.* **2017**, *383*, 467.
- [3] a) P. U. Jepsen, D. G. Cooke, M. Koch, *Laser Photonics Rev.* **2011**, *5*, 124; b) S. R. Murrill, E. L. Jacobs, S. K. Moyer, C. E. Halford, S. T. Griffin, F. C. De Lucia, D. T. Petkie, C. C. Franck, *Appl. Opt.* **2008**, *47*, 1286.
- [4] M. R. Leahy-Hoppa, M. J. Fitch, R. Osiander, *Anal. Bioanal. Chem.* **2009**, *395*, 247.
- [5] a) F. Wang, D. Zhao, H. Dong, L. Jiang, Y. Liu, S. Li, *Spectrochim. Acta, Part A* **2017**, *179*, 255; b) C. Yu, S. Fan, Y. Sun, E. Pickwell-MacPherson, *Quant. Imaging Med. Surg.* **2012**, *2*, 33.
- [6] a) I. F. Akyildiz, J. M. Jornet, C. Han, *Phys. Commun.* **2014**, *12*, 16; b) J. Federici, L. Moeller, *J. Appl. Phys.* **2010**, *107*, 111101; c) C. Han, A. O. Bicen, I. F. Akyildiz, *IEEE Trans. Wireless Commun.* **2015**, *14*, 2402.
- [7] R. E. McIntosh, R. M. Narayanan, J. B. Mead, D. H. Schaubert, *IEEE Trans. Microwave Theory* **1988**, *36*, 994.
- [8] R. W. McMillan, C. W. Trussell, R. A. Bohlander, J. C. Butterworth, R. E. Forsythe, *IEEE Trans. Microwave Theory* **1991**, *39*, 555.
- [9] L. Schrottke, X. Lü, G. Rozas, K. Biermann, H. T. Grahm, *Appl. Phys. Lett.* **2016**, *108*, 102102.
- [10] a) X. He, N. Fujimura, J. M. Lloyd, K. J. Erickson, A. A. Talin, Q. Zhang, W. Gao, Q. Jiang, Y. Kawano, R. H. Hauge, F. Léonard, J. Kono, *Nano Lett.* **2014**, *14*, 3953; b) D. Spirito, D. Coquillat, S. L. D. Bonis, A. Lombardo, M. Bruna, A. C. Ferrari, V. Pellegrini, A. Tredicucci, W. Knap, M. S. Vitiello, *Appl. Phys. Lett.* **2014**, *104*, 061111.
- [11] a) H. Tao, N. I. Landy, C. M. Bingham, X. Zhang, R. D. Averitt, W. J. Padilla, *Opt. Exp.* **2008**, *16*, 7181; b) F. Alves, B. Kearney, D. Grbovic, N. V. Lavrik, G. Karunasiri, *Appl. Phys. Lett.* **2012**, *100*, 111104; c) H. Tao, C. M. Bingham, A. C. Strikwerda, D. Pilon, D. Shrekenhamer, N. I. Landy, K. Fan, X. Zhang, W. J. Padilla, R. D. Averitt, *Phys. Rev. B* **2008**, *78*, 241103.
- [12] a) Q.-Y. Wen, H.-W. Zhang, Y.-S. Xie, Q.-H. Yang, Y.-L. Liu, *Appl. Phys. Lett.* **2009**, *95*, 241111; b) Y. Wen, W. Ma, J. Bailey, G. Matmon, X. Yu, G. Aeppli, *Appl. Opt.* **2013**, *52*, 4536; c) B.-X. Wang, X. Zhai, G.-Z. Wang, W.-Q. Huang, L.-L. Wang, *J. Appl. Phys.* **2015**, *117*, 014504.
- [13] X. Shen, Y. Yang, Y. Zang, J. Gu, J. Han, W. Zhang, T. J. Cui, *Appl. Phys. Lett.* **2012**, *101*, 154102.
- [14] S. Liu, H. Chen, T. J. Cui, *Appl. Phys. Lett.* **2015**, *106*, 151601.
- [15] a) T.-I. Jeon, K.-J. Kim, C. Kang, I. H. Maeng, J.-H. Son, K. H. An, J. Y. Lee, Y. H. Lee, *J. Appl. Phys.* **2004**, *95*, 5736; b) R. C. Che, L. M. Peng, X. F. Duan, Q. Chen, X. L. Liang, *Adv. Mater.* **2004**, *16*, 401.
- [16] a) M. A. Seo, J. W. Lee, D. S. Kim, *J. Appl. Phys.* **2006**, *99*, 066103; b) Y. Deng, Q. Sun, J. Yu, Y. Lin, J. Wang, *Opt. Exp.* **2013**, *21*, 5737.
- [17] a) H. Yan, X. Li, B. Chandra, G. Tulevski, Y. Wu, M. Freitag, W. Zhu, P. Avouris, F. Xia, *Nat. Nanotechnol.* **2012**, *7*, 330; b) K. Batrakov, P. Kuzhir, S. Maksimenko, N. Volynets, S. Voronovich, A. Paddubskaya, G. Valusis, T. Kaplas, Y. Svirko, P. Lambin, *Appl. Phys. Lett.* **2016**, *108*, 123101; c) J. M. Dawlaty, S. Shivaraman, J. Strait, P. George, M. Chandrashekar, F. Rana, M. G. Spencer, D. Veksler, Y. Chen, *Appl. Phys. Lett.* **2008**, *93*, 131905.
- [18] a) J. Zhao, W. Ren, H.-M. Cheng, *J. Mater. Chem.* **2012**, *22*, 20197; b) J. Chen, K. Sheng, P. Luo, C. Li, G. Shi, *Adv. Mater.* **2012**, *24*, 4569; c) Z. Xu, Y. Zhang, P. Li, C. Gao, *ACS Nano* **2012**, *6*, 7103; d) Z. Chen, W. Ren, L. Gao, B. Liu, S. Pei, H.-M. Cheng, *Nat. Mater.* **2011**, *10*, 424; e) Y. Zhao, J. Liu, Y. Hu, H. Cheng, C. Hu, C. Jiang,

- L. Jiang, A. Cao, L. Qu, *Adv. Mater.* **2013**, 25, 591; f) Y. Xu, K. Sheng, C. Li, G. Shi, *ACS Nano* **2010**, 4, 4324.
- [19] Y. Zhang, Y. Huang, T. Zhang, H. Chang, P. Xiao, H. Chen, Z. Huang, Y. Chen, *Adv. Mater.* **2015**, 27, 2049.
- [20] Y. Wu, N. Yi, L. Huang, T. Zhang, S. Fang, H. Chang, N. Li, J. Oh, J. A. Lee, M. Kozlov, A. C. Chipara, H. Terrones, P. Xiao, G. Long, Y. Huang, F. Zhang, L. Zhang, X. Lepró, C. Haines, M. D. Lima, N. P. Lopez, L. P. Rajukumar, A. L. Elias, S. Feng, S. J. Kim, N. T. Narayanan, P. M. Ajayan, M. Terrones, A. Aliev, P. Chu, Z. Zhang, R. H. Baughman, Y. Chen, *Nat. Commun.* **2015**, 6, 6141.
- [21] D. E. Aspnes, *Am. J. Phys.* **1982**, 50, 704.
- [22] S. Venkatachalam, D. Bertin, G. Ducournau, J. F. Lampin, D. Hourlier, *Carbon* **2016**, 100, 158.
- [23] J. H. Lehman, B. Lee, E. N. Grossman, *Appl. Opt.* **2011**, 50, 4099.
- [24] J. Zhu, Z. Ma, W. Sun, F. Ding, Q. He, L. Zhou, Y. Ma, *Appl. Phys. Lett.* **2014**, 105, 021102.
- [25] C. Shi, X. Zang, Y. Wang, L. Chen, B. Cai, Y. Zhu, *Appl. Phys. Lett.* **2015**, 117, 013101.
- [26] J. Lv, R. Y. Yuan, X. Song, H. Yan, *J. Appl. Phys.* **2014**, 105, 031104.
- [27] R. M. Gao, Z. C. Xu, C. F. Ding, J. Q. Ya, *Appl. Opt.* **2016**, 55, 1929.
- [28] X. Chen, W. Fan, *Appl. Opt.* **2015**, 54, 2376.
- [29] M. M. Jadidi, A. B. Sushkov, R. L. Myers-Ward, A. K. Boyd, K. M. Daniels, D. K. Gaskill, M. S. Fuhrer, H. D. Drew, T. E. Murphy, *Nano Lett.* **2015**, 15, 7099.
- [30] Y. Zhou, Y. E, Z. Ren, H. Fan, X. Xu, X. Zheng, D. Yuan Lei, W. Li, L. Wang, J. Bai, *J. Mater. Chem. C* **2015**, 3, 2548.